Nanoparticle–Size–Dependent Singlet Fission and Exciton Dynamics in Amorphous TIPS-Pentacene

Rohan J. Hudson, Alexandra N. Stuart, Jessica M. de la Perrelle, David M. Huang,* and Tak W. Kee*

Department of Chemistry, The University of Adelaide, Adelaide, South Australia, 5005, Australia

E-mail: david.huang@adelaide.edu.au; tak.kee@adelaide.edu.au

Phone: +61-(0)8-8313-5580; +61-(0)8-8313-5314

Abstract

Aqueous nanoparticle (NP) dispersions are commonly used as model systems for spectroscopic study of singlet exciton fission (SF) in acenes such as 6,13-(triisopropylsilylethynyl) pentacene (TIPS-Pn). However, the potential for particle size effects to complicate interpretation of results in such model systems is generally ignored. In this work, we study amorphous TIPS-Pn NP dispersions prepared by the re-precipitation method over a range of particle sizes. Time-resolved fluorescence and femtosecond transient absorption spectroscopy show that exciton dynamics in these systems depend significantly upon particle size. Kinetic analysis reveals that SF becomes slower at smaller NP sizes, while triplet exciton decay (through both correlated triplet pair relaxation and geminate triplet-triplet annihilation) accelerates. These significant size-dependent effects are ascribed to increased morphological disorder within smaller NPs, weakening the intermolecular couplings which control SF and triplet migration. A non-radiative singlet quenching channel separate from SF is also identified, which has not been previously reported for NPs of SF-capable chromophores. This non-radiative singlet decay becomes a significant relaxation pathway at small particle sizes, substantially reducing SF yields. Interestingly, exciton kinetics in 81-nm NPs approach those of bulk amorphous TIPS-Pn, suggesting that NPs of this size or larger are likely good models for bulk TIPS-Pn. This work demonstrates that particle-size effects are significant for small NPs of SF chromophores, and must be accounted for in order to accurately model bulk materials with such NP dispersions.

Introduction

Singlet exciton fission (SF) is an exciton multiplication process in which a chromophore in a singlet excited state (S_1) couples to a nearby ground-state chromophore to yield two lower-energy triplet excited state (T_1) chromophores.[1] This process is spin-allowed as it proceeds via a spin-0 correlated triplet pair intermediate ($^1(TT)$):[2,3]

$$S_1 + S_0 \rightarrow {}^1(TT) \rightarrow T_1 + T_1. \tag{1}$$

Interest in SF has risen dramatically in the last decade, as it has been recognised as a potential mechanism for improving photovoltaic (PV) device efficiencies beyond the theoretical efficiency limit for single-junction PV devices.[4–6] By forming two triplet excitons from every singlet exciton within the SF layer and subsequently harvesting these excitons, theoretical internal quantum efficiencies (IQEs) of 200% are possible for SF-sensitized PV devices. However, while SF-sensitized PV devices have been reported with IQEs surpassing 100%,[7,8] these devices remain much less efficient than conventional single-junction, inorganic PV architectures.[9,10] Significant effort is therefore being invested into improving understandings of how triplet excitons form and migrate in SF chromophores.

The known library of SF-capable compounds is highly diverse and has broadened substantially in recent years.[11,12] However, by far the most well-characterized class of SF chromophores are the acenes, especially pentacene and its derivatives, for which SF is exoergic and hence occurs quickly and irreversibly.[1,13] 6,13-(triisopropylsilylethynyl)pentacene (TIPS-Pn) in particular has attracted intensive study, as its bulky TIPS substituents improve solubility relative to unfunctionalized pentacene and facilitate an extended π-stacked motif in its predominant crystal polymorph.[14] Many different intermolecular packings for TIPS-Pn have since been reported: some studies have identified other crystal polymorphs,[15–17] while others have identified an amorphous phase.[18–22] TIPS-Pn is therefore widely considered a model system for intermolecular SF, as its wide variety of available morphologies allows for study

of the relationship between intermolecular packing and exciton dynamics.

Aqueous dispersions of TIPS-Pn nanoparticles (NPs) are commonly used for spectroscopic characterization of SF and associated exciton dynamics.[18,21,23–25] Study of NP dispersions allows solid-state photophysical processes to be probed while using liquid-phase samples, which minimizes experimental issues associated with the study of thin films and other solid-phase media such as photo-bleaching or sample opacity. Such dispersions are generally prepared through the "re-precipitation" or "flash precipitation" method first reported by Matsuda and co-workers.[26] In this technique a solution of chromophore in a good solvent is rapidly mixed with a (miscible) poor solvent, inducing fast chromophore aggregation and hence NP nucleation. TIPS-Pn NPs prepared by the re-precipitation method have been shown to form with amorphous morphologies,[18,21] although more recent studies have since demonstrated methods of converting these to crystalline structures through use of chemical additives.[19,24] Particle sizes can be readily tuned by control of re-precipitation conditions such as chromophore concentration or solvent combination,[27,28] and TIPS-Pn NPs have been reported with diameters in the range of 30–160 nm.[23,29] However, despite this wide range of NP sizes used to study SF dynamics in TIPS-Pn, the potential influence of NP size upon exciton dynamics in this system has not yet been considered.

Size-dependent properties of NPs prepared by the re-precipitation method are known to occur for a variety of chromophore types. Conjugated polymer NPs have been demonstrated to exhibit strongly size-dependent absorption and emission profiles, attributed to molecules at the NP surface adopting a more disordered morphology than those in the particle interior.[30,31] More recently, SF in aqueously dispersed diketopyrrolopyrrole (DPP) NPs was shown to become substantially faster at smaller particle sizes.[32] This acceleration of SF was ascribed to polar water molecules at the NP surface stabilizing charge-transfer states, which are thought to act as intermediates in the SF process for DPP. Therefore, a precedent exists for surface effects and morphological changes as a function of particle size in NP dispersions of SF chromophores, which may influence SF and other exciton dynamics. However, the

dependence of SF and related excitonic processes upon particle size within TIPS-Pn is currently unknown. As NP dispersions are often used to model SF and other exciton dynamics for TIPS-Pn thin films or other bulk media, it is hence crucial to understand and quantify any such particle-size effects which may occur in TIPS-Pn NPs.

In this work, we use transient absorption (TA) and time-resolved fluorescence spectroscopy to study amorphous TIPS-Pn NPs prepared by the re-precipitation method, with diameters ranging from 30 to 80 nm. Ultrafast exciton kinetics in these systems are found to vary significantly with NP diameter: smaller particle sizes yield slower SF, faster ^{1}(TT) non-radiative decay and faster T_1 decay through geminate triplet-triplet annihilation (TTA). These results are consistent with the NPs adopting an increasingly disordered morphology at smaller NP sizes, highlighting that not all amorphous structures of TIPS-Pn can be considered equivalent. SF yields are also found to decrease substantially at smaller particle sizes, which we attribute to an additional non-radiative singlet decay channel. These results demonstrate that NP size must be explicitly considered when using TIPS-Pn NP dispersions to study exciton dynamics, as morphological constraints and additional decay pathways become significant at small particle sizes.

Methods

Materials

TIPS-Pn was used as received from Ossila. Water was purified by an 18.2-MΩ cm Millipak Milli-Q IQ-7000 Water Purification System fitted with a 0.22-µm filter. HPLC-grade tetrahydrofuran (THF; RCI Labscan) was freshly distilled before use.

Nanoparticle Preparation and Size Characterization

Aqueous suspensions of amorphous-phase TIPS-Pn NPs were prepared by re-precipitation from THF solution into water, as has been previously reported by our group and others.[18,19,21,23–25] Multiple parameters in the preparation procedure were carefully tuned to achieve the broad range of NP sizes studied in this work. However, the overall procedure remained similar for the preparation of each NP sample, and so here we describe this procedure in general terms, with Table 1 listing exact quantitative details of the procedure used for each NP size. A volume V_{THF} of TIPS-Pn dissolved in THF at concentration [TIPS-Pn] was rapidly injected into a volume of water $V_{\mathrm{H_2O}}$ upon vigorous stirring, using a syringe needle of diameter d_{S}. This procedure was repeated n times, with each fraction stirred for 5 minutes. The n fractions were then combined and concentrated under reduced pressure to a final TIPS-Pn concentration of 100 ppm. Each NP suspension was then filtered through a 0.2-µm syringe filter (Sartorius Minisart NML).

NP sizes were characterized by dynamic light scattering (DLS), using a Malvern Zetasizer Nano ZSP with a 633-nm laser source and a backscattering angle of 173 °. Resulting intensity-weighted size distributions of each NP suspension are shown in Section S1 of the Supporting Information (SI). To differentiate between NP samples, we hereafter refer to each sample by its z-average diameter (d_{NP}) measured by DLS, shown in the final column of Table 1.

Table 1: Preparation Conditions for Different-Sized TIPS-Pn NPs by Re-Precipitation of THF Solution into Water, with NP z-Average Diameters as Measured by Dynamic Light Scattering

[TIPS-Pn] (ppm)	V_{THF} (mL)	$V_{\mathrm{H_2O}}$ (mL)	d_{S} (mm)[a]	# Fractions (n)	d_{NP} (nm)[b]
20	3	15	0.55	5	32.5 ± 0.1
50	3	15	0.55	2	45.1 ± 0.6
510	0.2	10	0.90	3	63.1 ± 0.3
1020	0.2	10	0.90	1	81.2 ± 0.4

[a] Exterior diameter of syringe needle.

[b] Uncertainties are twice the standard error in the mean calculated from triplicate measurements of each sample.

Steady-State Spectroscopic Characterization

Steady-state absorption spectra were collected in a 1-cm path length quartz cuvette (Starna Cells 21-Q-2), using a Cary Varian 1E UV-visible spectrophotometer. Steady-state fluorescence spectra were collected in a 1-cm path length quartz cuvette (Starna Cells 3-Q) on a Shimadzu RF-6000 fluorescence spectrofluorometer, using an excitation wavelength of 590 nm and excitation/emission slit bandwidths of 5 nm. All NP samples were diluted to a TIPS-Pn concentration of 2 ppm for fluorescence measurements, such that sample absorbance across the wavelength range studied was less than 0.1.

Time-Resolved Spectroscopic Characterization

Time-resolved spectroscopic measurements were made using the output of a Ti:sapphire regenerative amplifier (Spectra Physics, Spitfire Pro XP 100F), generating laser pulses centered at 800 nm and 100 fs in duration at a 1 kHz repetition rate. An optical parametric amplifier (Light Conversion, TOPAS-C) was used to produce 590 nm light from the second harmonic of the signal.

Time-resolved fluorescence measurements were performed using a fluorescence spectrometer (Ultrafast Systems, Halcyone) configured in upconversion (UC) mode. A small fraction of the 800 nm amplifier output was used to generate the UC gate, by focusing onto a 0.4-mm sapphire crystal for sum-frequency generation. The 590-nm pump pulses were focused to a

full width at half-maximum of 561 µm at the sample position, with a pulse energy of 0.1 µJ. Transient absorption measurements were collected using a transient absorption spectrometer (Ultrafast Systems, Helios). 590-nm pump pulses had a spot size of 560 µm at the sample position, with pump fluences varying from 20 to 80 µJ cm^{-2}. White-light continuum probe pulses were generated by focusing the 800 nm amplifier output onto a 3.2-mm sapphire crystal, with a spectral coverage of 450–750 nm and spot size of 130 µm at the sample position. For both time-resolved fluorescence and absorption experiments, pump and gate/probe pulses were polarized at 54.7° (magic angle) relative to one another, in order to minimize polarization biases in the measurements. NP suspensions were constantly stirred while under irradiation, with negligible photo-degradation observed throughout the course of these experiments.

Results and Discussion

Steady-State Spectrophotometric Characterization

Figure 1 shows the steady-state absorption spectra of all TIPS-Pn NP sizes studied here, with the absorption spectrum of TIPS-Pn in THF solution shown for reference. All NP samples exhibit spectral features closely resembling those of the solution spectrum, displaying a clear series of vibronic transitions within the $S_1 \leftarrow S_0$ manifold from 500 nm to 650 nm and $S_3 \leftarrow S_0$ and $S_4 \leftarrow S_0$ electronic transitions at 440 nm and 420 nm, respectively.[33] The NP absorption spectra differ from the solution spectrum by only a slight red shift, indicating that only weak inter-chromophore coupling occurs in these NPs. We therefore assign these NPs as possessing amorphous morphologies, agreeing with multiple other studies of similar systems.[18,21,24] A raised baseline is apparent at shorter wavelengths for increasing NP size, consistent with increased Rayleigh scattering for these larger particles. However, a slight red shift is also observed for all absorption peaks upon increasing NP diameter (inset of Figure 1). This minor spectral shift suggests that the average chemical environment experienced by TIPS-Pn molecules within the NPs changes subtly with NP size.

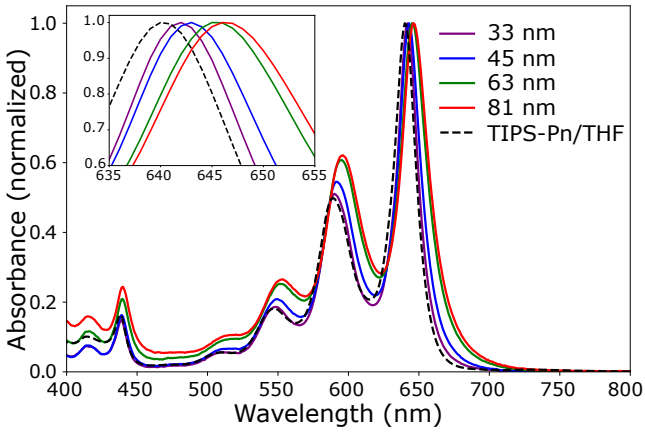

Figure 1: Steady-state absorption spectra of different-sized amorphous TIPS-Pn NPs, normalized to the $S_1 \leftarrow S_0$ 0–0 absorption peak around 645 nm. NP samples are labelled by diameter, and the steady-state absorption spectrum of TIPS-Pn in THF solution (dashed line) is shown for reference. Inset shows the shift in the position of the $S_1 \leftarrow S_0$ 0–0 absorption peak.

Steady-state fluorescence spectra of these NPs upon excitation at 590 nm are shown in Figure 2a, with pronounced 0–0 and 0–1 vibronic peaks evident at 650 nm and 710 nm, respectively. In contrast to the relatively similar absorption spectra displayed above, significant differences in the fluorescence spectra are observed upon changing NP size. Smaller TIPS-Pn NPs are much more fluorescent than larger NPs, with fluorescence intensity varying by over an order of magnitude across the particle sizes considered here. However, negligible changes in the overall spectral shape are observed upon varying NP size (SI, Section S2). Therefore, decreased emission intensity at larger particle sizes due to self-absorption within the NPs can be discounted, as self-absorption would result in a change in the intensity ratio of the 0–0 and 0–1 vibronic emission peaks. Time-resolved fluorescence can offer insight into the cause of this effective fluorescence quenching at larger NP sizes.

Time-Resolved Spectrophotometric Characterization

Time-resolved fluorescence upconversion (UC), detecting at 700 nm, was used to study the decay of the 0–1 emission band on the picosecond timescale. As is evident in Figure 2b, smaller TIPS-Pn NPs display much longer lived fluorescence at 700 nm than larger particles, thus accounting for the disparity in steady-state emission intensities. Fluorescence of larger NPs decays to baseline levels within 10 ps of excitation, whereas for smaller NPs some fluorescence intensity persists out to 50 ps (SI, Section S2). Radiative decay of singlet excitons in TIPS-Pn is known to occur on the order of tens of nanoseconds,[21] which is several orders of magnitude too slow to account for the very rapid decays observed here. Therefore, non-radiative decay of singlet excitons must be responsible for this variation in emission lifetime.

However, fluorescence detects only emissive singlet excitons here, and gives no information regarding the nature of the species formed by singlet decay. Therefore, to determine the cause of the observed rapid singlet exciton decay, a method capable of detecting non-emissive excitonic species must be used. To this end, we characterized our NP samples using transient

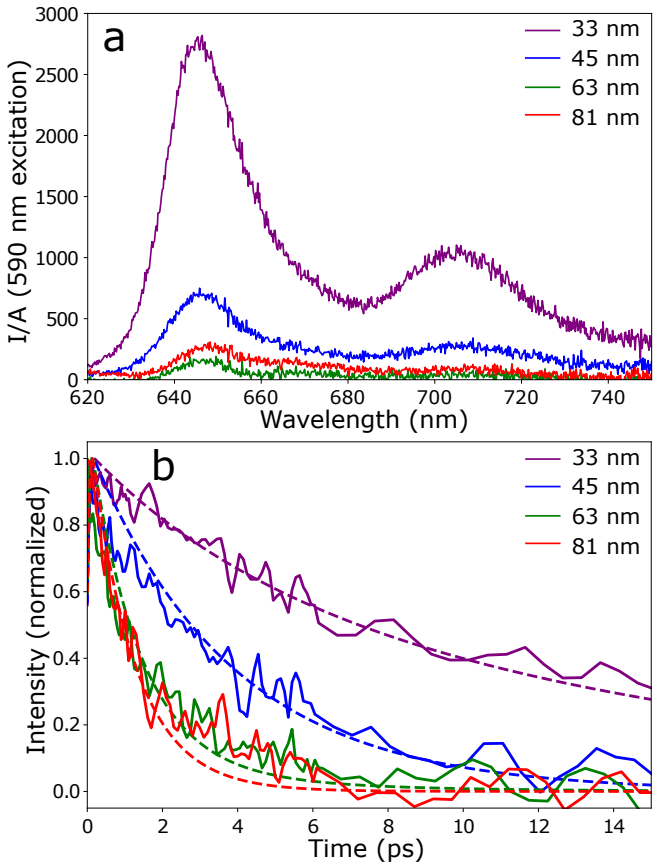

Figure 2: (a) Steady-state fluorescence spectra of amorphous TIPS-Pn nanoparticles, upon excitation at 590 nm. (b) Time-resolved fluorescence of TIPS-Pn NPs recorded at 700 nm, upon excitation at 590 nm. Dashed lines show fits of the S_1 population to the kinetic model described in Figure 6. NP samples are labelled by diameter. Time-resolved fluorescence traces have been smoothed by a Savitzky-Golay filter, using a 3rd-order polynomial and a 5-datapoint moving window.

absorption spectroscopy, exciting at 590 nm and detecting over the range 440–750 nm. Figure 3a shows representative TA spectra from each NP size at a probe delay time of 1 ps. Negative signals in the range of 600–650 nm mirror the steady-state absorption peaks shown in Figure 1, and are hence assigned as ground-state bleach (GSB) signals. The GSB at 650 nm overlaps with a stimulated emission (SE) signal at 650 nm, with another SE feature evident at 710 nm. These SE signals persist for longer times upon decreasing NP size, consistent with the above observation that singlet excitons survive longer in smaller NPs. An excited-state absorption (ESA) signal at 450 nm appears at early times for all NP samples, which decays with kinetics very similar to the time-resolved fluorescence for these NPs (Figure 3b). This peak therefore

appears to arise from a singlet excited state in amorphous TIPS-Pn, which is consistent with assignments of this peak to an $S_n \leftarrow S_1$ transition in other studies.[18,19,21] Concurrent with the decay of the 450 nm peak is the rise of an additional ESA at 507 nm, which grows on the order of 5–20 ps and decays over the 3.2 ns experimental time window (Figure 3c). This signal is well known to correspond to a $T_n \leftarrow T_1$ transition in disordered TIPS-Pn,[34,35] and hence indicates the formation of triplet excitons in these NPs. Intersystem crossing (ISC) occurs in TIPS-Pn on a timescale of 10^4–10^6 ps,[36] which is several orders of magnitude slower than the picosecond-scale rise of the triplet ESA signal observed here. Such rapid formation of triplet excitons therefore confirms that SF is responsible for some of the fast non-radiative decay of singlet excitons in these NPs. This assignment agrees with several previous studies which have reported SF occurring on timescales of 1–5 ps in amorphous TIPS-Pn.[18,19,21,22,24,35]

Upon decreasing NP diameter, the slower decay of singlet excitons noted above (Figures 2b and 3b) is coincident with a slower formation of the triplet ESA at 507 nm (inset of Figure 3c). This trend indicates that the overall rate of SF in these amorphous TIPS-Pn NPs depends upon NP size, with slower SF in smaller NPs. The decay of the triplet ESA signal also appears to vary significantly with NP size, as shown in Figure 3c. Within the observable 3.2 ns window, this ESA decays by only 22% for the 81-nm NPs but almost 40% for the smaller 33 nm sample. Clearly, NP size has a profound impact upon a number of excitonic processes within amorphous TIPS-Pn. However, it is difficult to precisely quantify these changes from the raw TA data shown here, as there is significant spectral overlap between the different exciton species in the visible region. The 450 nm ESA also contains a contribution from the triplet state, as evidenced by this signal not decaying to zero but plateauing at 30% of its initial intensity (Figure 3b). Additionally, several previous studies of amorphous TIPS-Pn have reported the correlated triplet-pair intermediate ^{1}(TT) to have a spectral signature distinct to that of free triplets in TIPS-Pn, with broad absorption features in the range of 400–600 nm and 700–800 nm.[19,21,37,38] Such absorption would overlap with the identified ESA signals of both singlet and triplet excitons, as well as the 0–1 SE signal

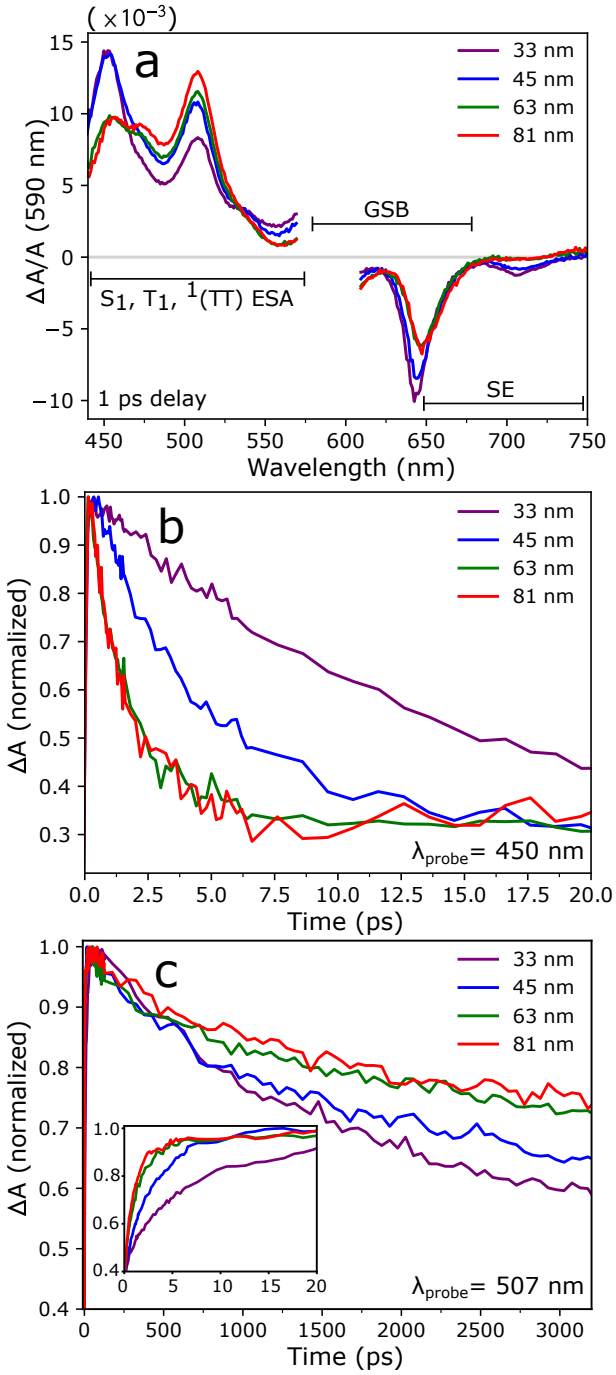

Figure 3: (a) Transient absorption spectra at 1 ps delay of amorphous TIPS-Pn NPs. Excited-state absorption (ESA), ground-state bleach (GSB) and stimulated emission (SE) features are labelled for clarity. (b) Early-time normalized kinetic traces of the 450 nm ESA, known to arise from singlet excitons in TIPS-Pn. (c) Normalized kinetic traces of the 507 nm ESA, attributed to triplet and triplet-pair excitons. Inset in (c) shows the 507 nm ESA kinetics over the first 20 ps after excitation. NP samples are labelled by diameter.

from the singlet state. As identified above, the 0–0 SE signal overlaps with the GSB at 650 nm, and the 0–1 GSB signal at 590 nm may be biased due to scattering of the 590 nm pump pulse and therefore unsuitable for analysis. As such, all TA spectral features identified here have contributions from either multiple exciton species or signals, and so use of single-wavelength kinetic traces to quantify the dynamics of SF and other processes in these NPs would be misleading. In order to more accurately quantify the impact of particle size upon the exciton dynamics in these NPs, the TA spectra presented above were decomposed into single-component contributions through the identification of exciton basis spectra.

Spectral Deconvolution of Transient Absorption Data

TA spectra are commonly deconvoluted using global and target analysis (GTA),[18,19,38] in which species-associated basis spectra may be extracted from a specified kinetic scheme. While GTA is a powerful analysis technique, it requires prior knowledge or assumptions of the underlying kinetic processes occurring in the system.[39] As the cause of the particle-size dependence upon singlet and triplet kinetics here is unclear, we deemed it necessary to deconvolute the TA spectra using a different method that is independent of any kinetic scheme. Instead of GTA, we used a method that we recently reported in a study of TIPS-Pn:poly(methyl methacrylate) (PMMA) composite NPs.[21] This method is summarized below, with resulting basis spectra for the various exciton species present shown in Figure 4a. The S_1 basis spectrum was extracted from TA spectra of a 1:90 TIPS-Pn:PMMA NP sample, for which singlet excitons dominate the spectra at early times, as the TIPS-Pn molecules are sufficiently dilute that SF is slow. The T_1 spectrum was determined from the 63-nm NP TA spectra at a long delay time of 3 ns, at which all S_1 excitons have undergone complete decay. Further details on the determination of each basis spectrum are given in Section S3 of the SI.

Many previous TA studies of pentacene derivatives have demonstrated that the intermediate ^{1}(TT) state has a spectral signature in the visible region distinct from free triplets,

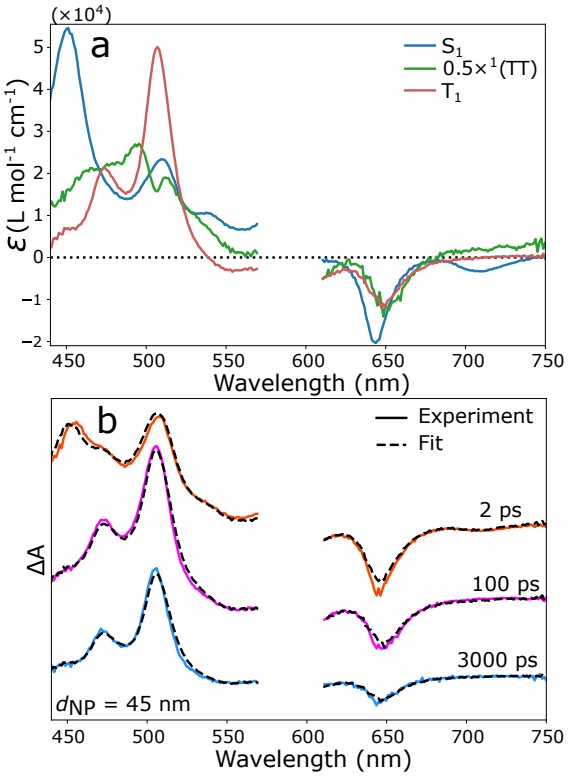

Figure 4: (a) Basis spectra of S_1, T_1 and ^{1}(TT) excitons in amorphous TIPS-Pn used to deconvolute the TA spectra here. (b) Fits to the TA spectra of the 45 nm diameter TIPS-Pn NPs using these basis spectra, at three representative delay times. The ^{1}(TT) basis spectrum shown in (a) uses $p = 0.1$, which was used in the deconvolution show in (b).

which must be accounted for in order to accurately describe the shape of TA spectra on the picosecond timescale.[19–21,37,40] We also calculated a ^{1}(TT) basis spectrum to be used in the spectral deconvolution here. Determination of this basis spectrum is more complex than for the S_1 and T_1 basis spectra, as ^{1}(TT) is an intermediate species and therefore always coexists with either singlet or triplet excitons in our NP samples. Triplet pair states in pentacene derivatives have been shown to form on timescales of 0.1–10 ps, and persist for up to nanoseconds in some circumstances.[19,21,40] Therefore, the ^{1}(TT) basis spectrum was determined here from the 63-nm NP TA spectra at a delay time of 10 ps, at which all S_1 excitons have decayed (Figure 2b) but both ^{1}(TT) and T_1 excitons are present. This extraction requires the assumption of a proportion of T_1 decay over the experimental time window, which is denoted p. The 507 nm ESA for the 63 nm NP sample decays by 25% over

the 3.2 ns window observed here, giving an upper bound of $p \approx 0.25$. Spectral deconvolution and kinetic fits shown in Figures 4–5 use an intermediate value of $p = 0.1$, but fits at $p = 0$ and $p = 0.25$ were used as upper and lower bounds for quantitative results presented in Table 2 and Figure 7.

TA data for each NP sample were deconvoluted by a linear combination fit of the three basis spectra $\epsilon_i(\lambda)$ to the data $\Delta A(t, \lambda)$ according to the Beer-Lambert law,

$$\Delta A(t, \lambda) = l \left([\mathrm{S_1}](t)\epsilon_{\mathrm{S_1}}(\lambda) + [^1(\mathrm{TT})](t)\epsilon_{^1(\mathrm{TT})}(\lambda) + [\mathrm{T_1}](t)\epsilon_{\mathrm{T_1}}(\lambda) \right), \tag{2}$$

where l is the path length and square brackets denote concentrations. Figure 4b shows representative spectral fits for the 45-nm NP sample, with fits for all other NP sizes shown in Section S4 of the SI. This three-component fit results in excellent reconstruction of the TA data across the entire time window and range of NP sizes, capturing all of the GSB, SE and ESA signals identified above. Exciton concentrations extracted from this deconvolution for 33-nm and 81-nm NPs are shown in Figure 5, with concentrations for all NP samples shown in Section S4 of the SI. The trends identified from the TA data are reproduced in these extracted concentrations: larger NP sizes show faster SF and slower free triplet decay. Additionally, decay of ^{1}(TT) excitons appears to occur more rapidly in smaller NPs; as shown in Figure 5, the triplet pair population decays almost to zero after 500 ps for the 33-nm NPs, but a significant population of ^{1}(TT) still exists at this time for the larger 81-nm NPs. Clearly, NP size has a considerable influence upon the dynamics of $\mathrm{S_1}$, $\mathrm{T_1}$ and ^{1}(TT) excitons in amorphous TIPS-Pn.

In addition to the exciton kinetics identified above, another feature of considerable interest is the yield of the SF process. A SF yield close to 2 (often termed "quantitative SF") is frequently identified as one of the most necessary aspects for SF-capable PV devices to circumvent the detailed-balance limit.[1,6] However, the precise definition of the SF yield is not consistent in the literature. Some studies consider only the yield of the initial

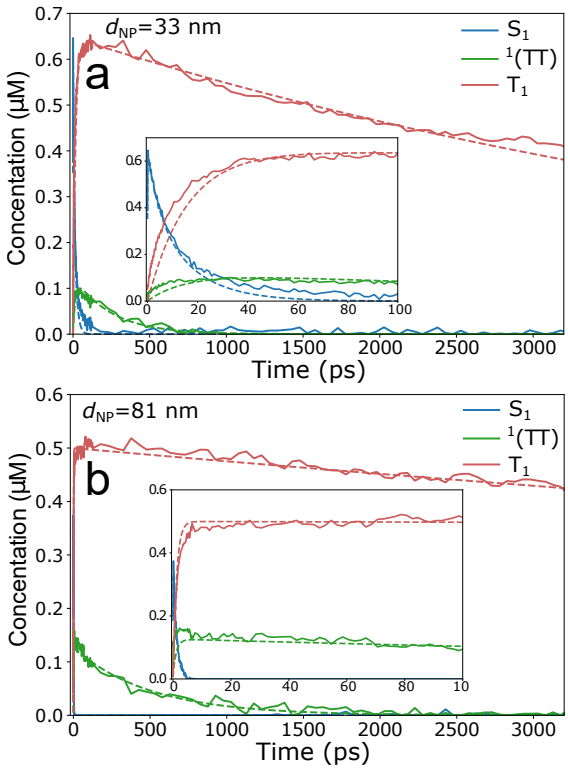

Figure 5: Extracted exciton concentrations from spectral deconvolution (solid lines) and kinetic fits to the model described in Figure 6 (dashed lines) for (a) 33-nm and (b) 81-nm TIPS-Pn NPs. Insets show the same data on a shorter timescale of 100 ps after excitation. Spectral deconvolution shown here used a ^{1}(TT) basis spectrum taken using $p = 0.1$.

$S_1 + S_0 \rightarrow {}^1(TT)$ step,[18,23] while others define the SF yield as the total yield of free triplet excitons.[1] We consider both definitions here, defining the overall SF quantum yield ϕ_{SF} as

$$\phi_{SF} = \frac{\max([T_1])}{\max([S_1])}, \tag{3}$$

while the yield including the first SF step ϕ'_{SF} is given by

$$\phi'_{SF} = \frac{\max([T_1] + 2 \times [{}^1(TT)])}{\max([S_1])}. \tag{4}$$

Table 2 shows ϕ_{SF} and ϕ'_{SF} for all NP sizes considered here, determined from exciton concentrations extracted from spectral deconvolution. ϕ'_{SF} is consistently larger than ϕ_{SF} for all NP sizes, indicating that not all ^{1}(TT) states formed during SF separate into free triplets. Other

studies of various pentacene derivatives have demonstrated that triplet-pair states formed from SF can undergo non-radiative decay to the ground state.[20,21,40] A slow decay of the ^{1}(TT) population over hundreds of picoseconds is observed here for all NP sizes, as shown in Figure 5 and Section S4 of the SI. Therefore, it is likely that such non-radiative ^{1}(TT) decay also occurs here, reducing the total yield of T_1 excitons from SF. This ^{1}(TT) decay cannot be explained by recombination of triplet pairs into singlet excitons, as the singlet population fit by spectral deconvolution remains at zero during the slow decay of correlated triplet pairs.

Table 2: Overall SF Quantum Yields (ϕ_{SF}) and Yields of the First SF Step (ϕ'_{SF}) Determined from Spectral Deconvolution of TA Data [a]

d_{NP} (nm)	ϕ_{SF}	ϕ'_{SF}
33	1.03±0.05	1.26±0.03
45	1.2±0.1	1.65±0.01
63	1.3±0.1	1.85±0.01
81	1.5±0.1	2.05±0.01 [b]

[a] Values are averages for fits at $p = 0$ and $p = 0.25$. Uncertainties represent the range of fit values between $p = 0$ and $p = 0.25$.

[b] SF is sufficiently fast in this sample that the singlet population decays appreciably within the TA instrument response function of 150 fs. This results in an under-estimate of max([S_1]) from spectral deconvolution and hence yields ϕ'_{SF} slightly greater than 2.

Interestingly, a clear trend can be discerned for both ϕ'_{SF} and ϕ_{SF}, with both yields increasing as a function of NP size. ϕ'_{SF} is approximately 2 for the 81-nm NPs, indicating that the first step of SF is quantitative for these larger particles. This result agrees with previous work that estimated unity yield from the $S_1 + S_0 \rightarrow {}^1$(TT) step in 70-nm diameter amorphous TIPS-Pn NPs.[19] Lower ϕ'_{SF} are observed at smaller particle sizes, however, indicating that some singlet excitons decay without forming triplet pairs. Rapid decay of triplet and triplet pair excitons cannot account for such significant reductions in yield; estimation of the ^{1}(TT) decay rate indicates that fast non-radiative triplet pair decay could reduce ϕ'_{SF} to a minimum value of 1.64 for the 33-nm NPs (SI, Section S5), which is significantly higher than the measured value of 1.26. Therefore, these results suggest that an additional singlet decay

pathway may exist in parallel to SF, which becomes significant at smaller NP sizes. This pathway would result in an additional reduction of the singlet population without forming T_1 or $^1(TT)$ excitons, hence decreasing both ϕ'_{SF} and ϕ_{SF}.

Kinetic Analysis of Transient Absorption Data

Kinetic Model

In order to explain the complex dependence of exciton dynamics upon NP size observed here, we used a kinetic model to fit the extracted exciton concentrations, described schematically in Figure 6. This model consists of two populations of singlet excitons, two populations of triplet pair excitons, and one population of triplet excitons. One population of singlet excitons ($S_{1,SF}$) undergoes SF through two competing pathways, forming triplet pair populations $^1(TT)_A$ and $^1(TT)_B$. This split population of triplet pairs is necessary to describe the non-radiative $^1(TT)$ decay identified above, as a single $^1(TT)$ population cannot accommodate both fast separation into T_1 excitons and long-lived $^1(TT)$ excitons over hundreds of picoseconds. Therefore, the model used here splits the population of triplet pairs into $^1(TT)_A$, which do not separate but decay non-radiatively with rate coefficient k_{pair}; and $^1(TT)_B$, which separate into free triplet excitons with rate constant k_{sep}. These triplet pair populations are formed from $S_{1,SF}$ with rate coefficients $k_{SF,A}$ and $k_{SF,B}$, respectively. T_1 excitons decay to the ground state with coefficient k_T. All of these aspects are consistent with the model used in our previous study of TIPS-Pn:PMMA composite NPs.[21] However, to account for the low ϕ'_{SF} and ϕ_{SF} at small NP sizes shown in Table 2 we have also included an additional singlet population, termed $S_{1,NR}$. As mentioned above, this singlet population undergoes non-radiative decay directly to the ground state, with rate coefficient k_{NR} in the model. The fraction of singlet excitons in this $S_{1,NR}$ population is given by the parameter f_{NR}, which was fit for each NP size. As discussed below, including this additional singlet population is necessary to obtain a good fit the data. Radiative decay of the singlet state is ignored in this model; as mentioned above this process is known to occur on a timescale on

the order of 10 ns and should therefore be negligible on the timescale considered here.[21] We have also disregarded diffusive transport between singlet populations, as estimated singlet diffusion lengths indicate that minimal diffusion occurs before the S_1 state is fully depopulated (SI, Section S6). The resulting kinetic model can be described by a series of coupled differential equations:

$$\begin{aligned}
\frac{\mathrm{d}[\mathrm{S}_{1,\mathrm{SF}}]}{\mathrm{d}t} &= -(k_{\mathrm{SF,A}} + k_{\mathrm{SF,B}})[\mathrm{S}_{1,\mathrm{SF}}]; \\
\frac{\mathrm{d}[\mathrm{S}_{1,\mathrm{NR}}]}{\mathrm{d}t} &= -k_{\mathrm{NR}}[\mathrm{S}_{1,\mathrm{NR}}]; \\
\frac{\mathrm{d}[^1(\mathrm{TT})_{\mathrm{A}}]}{\mathrm{d}t} &= k_{\mathrm{SF,A}}[\mathrm{S}_{1,\mathrm{SF}}] - k_{\mathrm{pair}}[^1(\mathrm{TT})_{\mathrm{A}}]; \\
\frac{\mathrm{d}[^1(\mathrm{TT})_{\mathrm{B}}]}{\mathrm{d}t} &= k_{\mathrm{SF,B}}[\mathrm{S}_{1,\mathrm{SF}}] - k_{\mathrm{sep}}[^1(\mathrm{TT})_{\mathrm{B}}]; \\
\frac{\mathrm{d}[\mathrm{T}_1]}{\mathrm{d}t} &= 2k_{\mathrm{sep}}[^1(\mathrm{TT})_{\mathrm{B}}] - k_{\mathrm{T}}[\mathrm{T}_1].
\end{aligned} \tag{5}$$

The system described by eq 5 and Figure 6 was solved numerically and fit to the extracted exciton concentrations by an iterative least-squares method. $k_{\mathrm{SF,A}}$, $k_{\mathrm{SF,B}}$, f_{NR}, k_{pair} and k_{T} were allowed to vary with NP size. k_{sep} and k_{NR} were found to be effectively independent of NP diameter, and so were fit to constant values across all NP sizes. Best-fit parameters to this model are shown in Figure 7, with fits to the 33-nm and 81-nm NP data shown in Figure 5. Fits to all NP sizes are shown in Section S7 of the SI. A relatively good fit to the data is observed for all NP sizes, suggesting that this model provides a reasonable description of the underlying physical processes occurring in these systems. The only discrepancy in this fit is an over-estimation of the singlet decay at later times in the 33-nm NPs, as evident in the inset of Figure 5a. This discrepancy may be due to the presence of trap sites in this system (sites at which excitons cannot move or decay), which have previously been reported for both pentacene and TIPS-Pn but are not taken into account in the kinetic model used here.[21,23,41] However, this model still adequately describes the majority of singlet decay in the 33-nm NPs, and so this minor disagreement likely has an insignificant impact on the

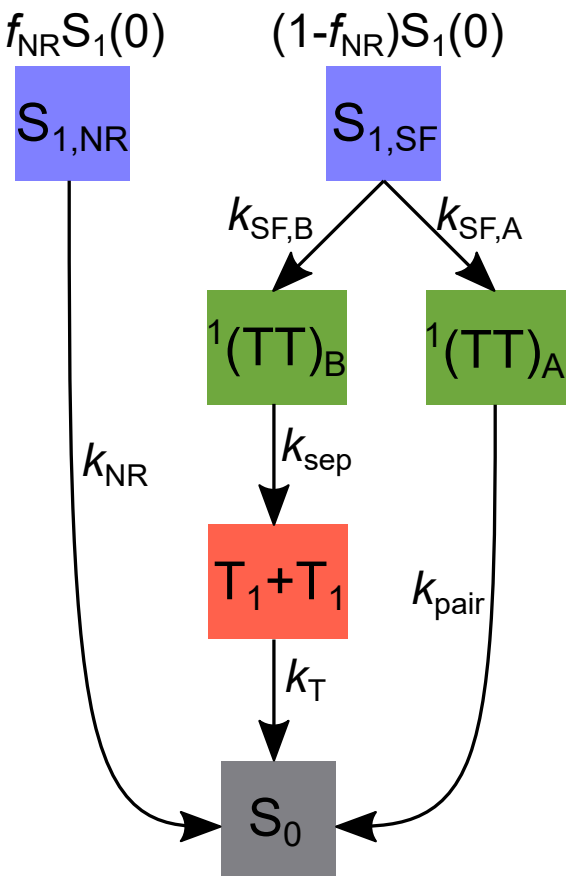

Figure 6: Schematic diagram of the kinetic model used to fit the TA data.

conclusions drawn from this analysis.

Size-Dependent Exciton Dynamics

Several trends are immediately evident from the fit parameters shown in Figure 7, which agree with the qualitative trends observed in the TA data mentioned above. On increasing NP diameter, rate coefficients of SF ($k_{\mathrm{SF,A}}$ and $k_{\mathrm{SF,B}}$) increase by over an order of magnitude, f_{NR} decreases to zero, k_{pair} decreases by half, and k_{T} decreases by almost a factor of 3. f_{NR} decreases from almost one-third to effectively zero across the NP sizes studied here, consistent with the increase in ϕ'_{SF} with NP size shown in Table 2 and the quantitative yield noted for the 81-nm NPs. SF time constants, $\tau_{\mathrm{SF}} = (k_{\mathrm{SF,A}} + k_{\mathrm{SF,B}})^{-1}$, range from 15 ps for the smallest NPs to 1.3 ps for the 81-nm NPs. The latter value agrees closely with SF time constants previously reported for amorphous TIPS-Pn films,[22,35] suggesting that these larger

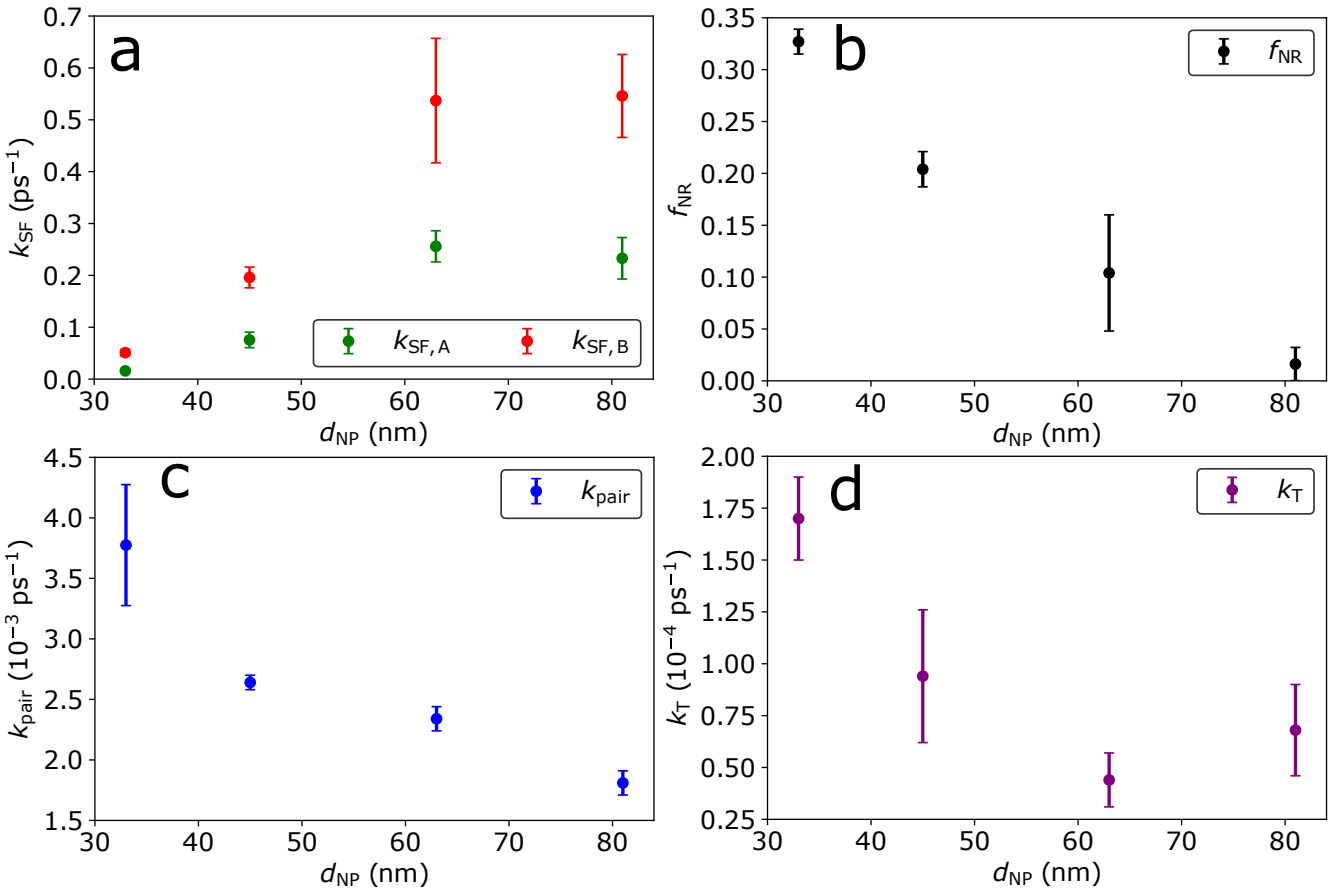

Figure 7: Best-fit values of (a) $k_{SF,A}$ and $k_{SF,B}$, (b) f_{NR}, (c) k_{pair} and (d) k_T from the kinetic model described in Figure 6 for all NP sizes. k_{sep} and k_{NR} fit to constant values across all NP sizes of $20.0 \pm 0.5\,\mathrm{ps}^{-1}$ and $0.17 \pm 0.03\,\mathrm{ps}^{-1}$, respectively. Values are averages for fits at $p = 0$ and $p = 0.25$, and uncertainties represent the range of fit values between $p = 0$ and $p = 0.25$.

NPs exhibit SF kinetics similar to those of bulk TIPS-Pn. Best-fit values of k_{pair} are also of a similar order of magnitude to rate coefficients of ^{1}(TT) decay reported for TIPS-Pn[19,21] and other acene materials.[20,40]

However, the best-fit values of k_T determined here are 2–3 orders of magnitude larger than the rate coefficient for natural first-order decay of T_1 excitons, which has been demonstrated to be on the order of $10^{-7}\,\mathrm{ps}^{-1}$.[22] Therefore, it is unlikely that the change in k_T with NP size here arises from natural triplet decay. Neither bimolecular TTA nor triplet-charge annihilation at the NP surface is consistent with this relatively fast T_1 decay, as varying either the excitation density or NP surface charge have negligible effects upon the observed

triplet decay kinetics (SI, Section S8). Therefore, the likely cause of this fast triplet decay is geminate TTA, in which pairs of triplet excitons generated from the same SF event annihilate with pseudo-first-order kinetics. We stress that is an annihilation process rather than recombination to the S_1 state, as neither re-formation of the singlet state in the TA spectra or delayed fluorescence occur in the results presented here. This lack of singlet re-formation is unsurprising, given that the $T_1 + T_1 \rightarrow S_1 + S_0$ process is endoergic in TIPS-Pn and therefore unfavorable.[1] For geminate annihilation to be the dominant triplet decay pathway here, separated triplet excitons must remain trapped in relatively close proximity to one another. A poor triplet exciton mobility is hence expected for these NPs, which is supported by a previous study of amorphous TIPS-Pn films.[22] Estimated triplet diffusion coefficients from this previous study correspond to diffusion lengths of less than 1 nm on the timescale of this experiment (SI, Section S6). This diffusion length equates to an intermolecular separation of only 1–2 TIPS-Pn molecules, depending upon relative molecular orientations.[14] Several recent studies of both amorphous and crystalline TIPS-Pn have included a spin-correlated but spatially-separated (T$\cdots$T) state as an intermediate between ^{1}(TT) and $T_1 + T_1$ in their description of triplet pair separation, which is assigned as being spectrally indistinguishable from free triplet excitons.[17,20,35] Given the poor triplet mobility and significant geminate TTA observed here, a significant population of T_1 excitons here may hence exist as (T$\cdots$T) exciton pairs, separated only by 1–2 molecules. However, geminate annihilation of either free triplet excitons or (T$\cdots$T) pairs would result in first-order decay with respect to triplet concentration,[20,42,43] and so the results presented here cannot distinguish between these processes. Despite this, these data clearly show that geminate annihilation of triplet excitons accelerates at smaller particle sizes, concurrent with slower SF and faster ^{1}(TT) relaxation.

Changes in Nanoparticle Morphology

Overall, the results of this kinetic modelling show that SF becomes slower while non-radiative ^{1}(TT) decay and geminate TTA become faster as the diameter of amorphous TIPS-Pn NPs

decreases. As all of these processes involve intermolecular exciton interactions, it is reasonable to infer that these changes likely arise from variations in NP morphology with particle size. Previous studies have demonstrated that polymers such as PMMA or poly(vinyl alcohol) (PVA) can disrupt or alter the morphology of TIPS-Pn NPs,[21,24] while the use of other additives as surfactants or emulsifying agents has been shown to alter the intermolecular packing of other organic nanoaggregates.[44,45] However, as the preparation of the TIPS-Pn NPs studied here uses only water, THF and TIPS-Pn, these changes in dynamics are unrelated to other chemical species disrupting or changing the NP morphology. Therefore, any change in morphology with NP size can only be due to a variation of the inherent TIPS-Pn intermolecular packing. While all NP sizes show spectral characteristics consistent with an amorphous morphology, Figure 1 shows a slight shift in the 0–0 $S_1 \leftarrow S_0$ steady-state absorption peak upon changing NP size. Similar peak shifts in TIPS-Pn and other functionalized pentacene derivatives have been previously attributed to changes in intermolecular packing, with more blue-shifted spectral features ascribed to a less dense and more "solvent-like" intermolecular packing in the solid state.[20,21] The peak shift observed here may hence indicate that smaller TIPS-Pn NPs may have more disordered solid-state packings than larger NPs, which is consistent with the changes in exciton dynamics noted here. Therefore, while all NP sizes studied here possess morphologies that can be classed as amorphous, these morphologies contain differing levels of disorder and cannot be considered as equivalent. The first step of SF, $S_1 + S_0 \rightarrow {}^1(TT)$, depends strongly upon the electronic coupling strength between adjacent chromophores,[1] and so an increase in molecular disorder would reduce the coupling between neighboring molecules, slowing the average rate of SF. Greater disorder would also inhibit long-range separation of triplet excitons, as triplet hopping through Dexter energy transfer depends strongly upon interchromophore distance.[46,47] This restriction of exciton mobility would increase the probability of triplet excitons formed from the same SF event remaining in close proximity to one another, thereby increasing the rate of geminate TTA.

Separation of the triplet pair state into free triplets has been shown to be limited by triplet hopping away from the initial SF site in crystalline[37] and amorphous[21] TIPS-Pn. As mentioned above, an increase in molecular disorder would significantly slow triplet mobility in these NPs. Hence, a more disordered intermolecular packing in these NPs could potentially slow the overall rate of ^{1}(TT) separation. However, the kinetic analysis undertaken here indicates that the rate coefficient of triplet pair separation is independent of NP size, fitting to a constant value of k_{sep}=20 ps^{-1}. This value corresponds to ^{1}(TT) separation occurring on a timescale of <100 fs, which is over an order of magnitude faster than $^1(\text{TT})_{\text{B}}$ formation ($\tau_{\text{SF,B}} \approx 2 - 20$ ps). The model used here is therefore relatively insensitive to the value of k_{sep}, as the rate-limiting step for T_1 formation is the $S_1 + S_0 \rightarrow {}^1(\text{TT})$ step. Therefore, it is difficult to fit k_{sep} to a high level of accuracy with the kinetic model used here. Contrasting with this behavior for k_{sep}, k_{pair} shows a strong dependence upon NP size, becoming significantly larger at smaller NP sizes. The exact mechanism by which the triplet pair state decays non-radiatively is still unclear, and so it is difficult to justify this accelerated decay at smaller NP sizes. However, increased morphological disorder at smaller particle sizes likely corresponds to less rigidity in the intermolecular packing within the NPs. The corresponding greater degrees of freedom in molecular vibrations and other nuclear motions may increase mixing of electronic states responsible for this non-radiative decay.[48] The faster non-radiative ^{1}(TT) decay observed here at smaller particle sizes is therefore likely due to increased morphological disorder allowing greater degrees of freedom to the nuclear motions which facilitate this decay.

Singlet Exciton Quenching

The inclusion of a singlet population undergoing non-radiative decay in the kinetic model used here is intriguing. Kinetic fits to the TA data without this non-radiative decay pathway resulted in poor fits for the 33- and 45-nm NP samples (SI, Section S9), with the fitted triplet/triplet pair concentrations overly high for these smaller NPs. Inclusion of this addi-

tional non-radiative S_1 decay mechanism is hence necessary to adequately describe the T_1 and ^{1}(TT) kinetics for these smaller NPs. This result is consistent with the SF yields shown in Table 2, as the low values of ϕ'_{SF} reported here for smaller NPs suggest that a singlet decay pathway independent of SF must also be present in these systems. SF in amorphous TIPS-Pn has been extensively studied,[18–23,35] but this non-radiative, non-SF related pathway appears to have been identified here for the first time. However, all of these previous studies considered either thin films or relatively large NPs ($d_{NP} > 70$ nm). As shown in Figure 7b, f_{NR} decreases to nearly zero for the 81-nm NPs, indicating that this non-radiative decay pathway is effectively negligible for NPs of this size or larger. Therefore, this singlet quenching mechanism has likely not been reported before because it is only significant for relatively small NPs ($d_{NP} \leq 60$ nm), and was hence absent in the larger particles or bulk films used in previous studies.

Aqueous colloidal dispersions of acenes and other organic semiconductors are known to acquire a negative surface charge during the re-precipitation process,[24,30,45] and so we considered the possibility that this singlet quenching effect arises from singlet–charge annihilation at the NP surface. However, varying the NP surface charge density resulted in negligible changes to singlet decay kinetics in these NPs (SI, Section S8). Hence, it is unlikely that exciton–charge annihilation is the primary cause of this non-radiative decay. As the TA experiments conducted here were undertaken under standard atmospheric conditions, it is also possible that dissolved oxygen may contribute to exciton quenching at the NP surface. However, previous studies of acene quenching by triplet oxygen have measured rate coefficients on the order of 10^9–10^{10} s^{-1}, which is 1–2 orders of magnitude lower than the picosecond-scale S_1 deactivation observed here.[49,50] Therefore, singlet quenching by triplet oxygen is also unlikely to be the main cause of the non-radiative singlet decay observed here. Picosecond-scale non-radiative singlet decay in aqueously-dispersed fullerene NPs has previously been attributed to exciton quenching by water.[51] However, the authors of this prior work assigned this exciton decay as arising from water–exciton interactions without of-

fering comment on the underlying mechanism by which this might occur. Relatively strong exciton–water couplings would be required for water molecules to quench singlet excitons on such a fast timescale, presumably through interactions with the dipole moment of water molecules. Other studies have previously suggested that increased intermolecular coupling in pentacene derivatives is concurrent with increased charge-transfer (CT) nature of singlet excitons.[18] Such CT character in S_1 excitons could result in strong dipolar coupling to water molecules at the NP surface. However, the results presented here indicate that average TIPS-Pn intermolecular couplings become stronger with increasing NP size, which would therefore increase the CT character of singlet excitons in larger NPs. If singlet–water interactions were responsible for this non-radiative quenching, then larger particle sizes would hence be expected to yield stronger water–exciton couplings and therefore more singlet quenching at larger particle sizes. This is the opposite of the trend observed here for f_{NR}, and so quenching by water molecules is unlikely to be the physical cause of this non-radiative singlet exciton decay.

As the non-radiative singlet decay recorded here is unlikely to arise from exciton quenching by SF, surface charges, dissolved oxygen or water molecules, it is logical to consider that this process may be due to the inherent morphology of small TIPS-Pn NPs. The inverse scaling of f_{NR} with particle size could suggest that this morphology resides at the NP surface, as the NP surface area:volume ratio also scales inversely with d_{NP} (SI, Section S10). Surface morphologies that differ from those of the NP interior or the bulk material have been previously reported for conjugated polymer NPs, attributed to the curvature of the NP surface restricting intermolecular packing.[30,31] The non-radiative singlet decay observed here could hence be due to morphologies formed at the NP surface which are conducive to fast non-radiative exciton quenching. We considered a model in which singlet quenching may occur within a finite depth of the NP surface (SI, Section S10), which may explain the decrease of f_{NR} with particle size recorded here. However, the good fit of this model is not definitive evidence of this singlet quenching occurring solely at the NP surface; changes in morphology

throughout the entire NP volume could also explain the scaling of f_{NR}. Therefore, the exact physical cause of this non-radiative singlet quenching is unclear from the results presented here.

TIPS-Pn Nanoparticles as Models for Bulk Systems

Three pathways of exciton decay to the ground state in amorphous TIPS-Pn NPs have been identified here: non-radiative quenching of singlet excitons, relaxation of ^{1}(TT) intermediates unable to separate, and geminate annihilation of separated triplet excitons. All of these processes (illustrated in Figure 8) depend strongly on NP size, with rate coefficients or population fractions that vary by up to an order of magnitude across the sizes considered here. This apparent dependence upon NP size is likely due to variations in morphological disorder within the NPs, which becomes more significant at smaller particle sizes. This behavior may be due to geometric constraints; increased curvature at the NP surface at smaller sizes may restrict intermolecular packing within the particle, thus increasing disorder. Growth of NPs to larger sizes may allow for more reorganization within the NP, hence decreasing disorder in the overall intermolecular packing.

The strong size dependence of excitonic processes in amorphous TIPS-Pn NPs uncovered here may help to resolve some discrepancies in the literature. Munson and co-workers demonstrated that SF in amorphous TIPS-Pn films occurred on a sub-picosecond timescale,[35] but a recent study of small ($d_{\mathrm{NP}} = 30\,\mathrm{nm}$) amorphous NPs showed no detectable SF within a 500 fs window.[29] Recognizing that the NPs in the latter study were of comparable size to the smallest NPs used here, these NPs likely possessed significant morphological disorder due to their small size, causing SF to occur much more slowly than in the bulk film. Such varying degrees of disorder with NP size likely also accounts for the wide variety of SF rate coefficients for amorphous TIPS-Pn NPs in other studies, which vary by up to an order of magnitude.[18,19,21,23,29,35] Additionally, while the natural triplet lifetime in bulk TIPS-Pn is known to be on the order of µs,[22] other studies of amorphous TIPS-Pn NPs have reported

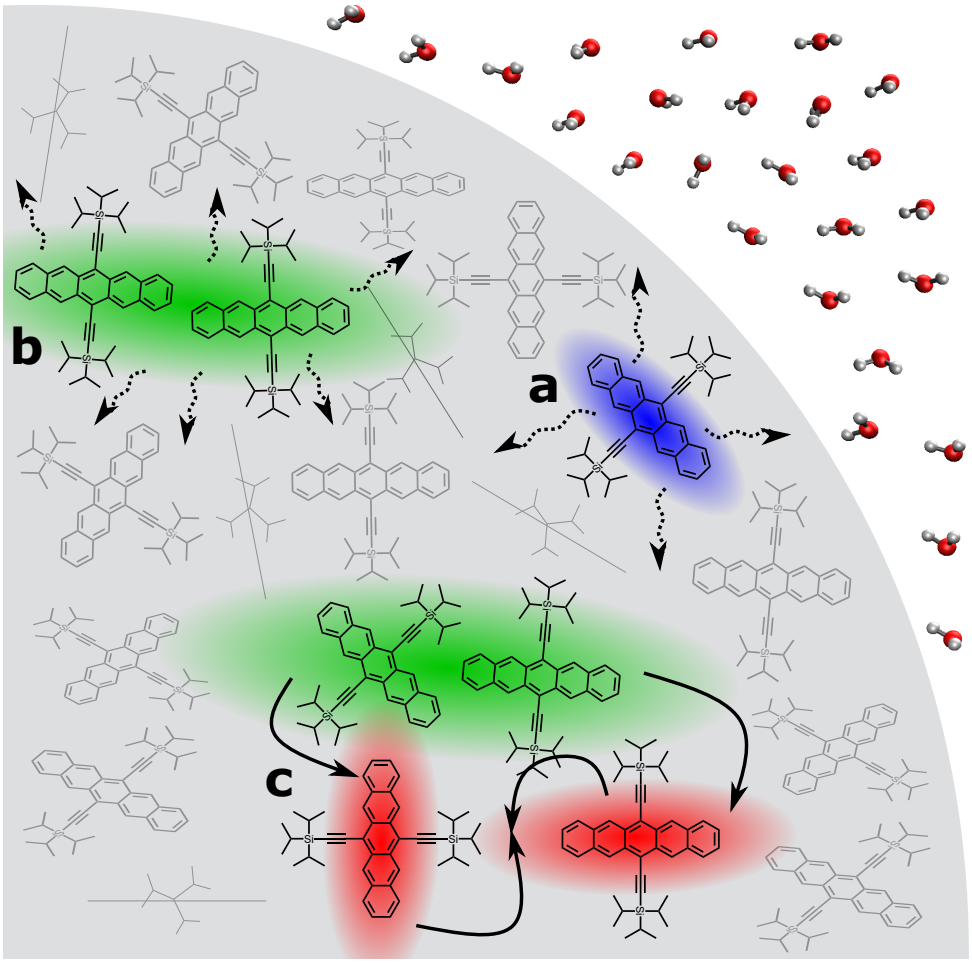

Figure 8: Illustration of the three different exciton decay pathways identified for amorphous TIPS-Pn NPs in this work: a) non-radiative singlet decay, b) non-radiative triplet pair decay, and c) triplet pair separation and subsequent geminate annihilation. Singlet excitons are shown in blue, triplet pair excitons in green and triplet excitons in red. Solid arrows denote exciton hopping and annihilation processes, while dashed arrows indicate non-radiative decay.

first-order triplet decay orders of magnitude faster than this.[21,23] Again, this disagreement is likely due to higher disorder in NPs relative to bulk films, inhibiting triplet mobility and hence resulting in fast geminate TTA. The results of the present study therefore demonstrate the need for caution when using NP dispersions as models for bulk systems. Particle size effects, exciton quenching or other NP-specific processes that are irrelevant in the bulk may be important in such systems. Although use of NPs as model systems can yield useful information regarding SF, particle size should be explicitly considered when designing studies using NP models. For the case of amorphous TIPS-Pn considered here, singlet exciton quenching and size-dependent exciton dynamics are most prevalent at smaller NP sizes. As shown in Figure 7, rate coefficients of all excitonic processes begin to converge for $d_{\mathrm{NP}} = 63$–$81\,\mathrm{nm}$, and f_{NR} reduces to effectively zero for the 81-nm NPs. Therefore, it can be reasonably concluded that particle-size-effects for amorphous TIPS-Pn NPs become negligible in the region of $d_{\mathrm{NP}} = 63$–$81\,\mathrm{nm}$, and hence NPs of this size or larger should be reasonable models for bulk amorphous TIPS-Pn.

Conclusions

This work has demonstrated that exciton dynamics in amorphous TIPS-Pn NPs depend significantly upon particle size. While steady-state spectral characteristics indicate that all NPs possess amorphous morphologies, transient absorption and time-resolved fluorescence results show substantial variation in the dynamics of both singlet and triplet excitons with particle size. Spectral deconvolution and kinetic analysis show that larger NPs exhibit faster SF, slower ^{1}(TT) non-radiative decay and slower free triplet decay through geminate annihilation. These results are consistent with the intermolecular packing in these NPs becoming more disordered at smaller particle sizes, slowing SF and triplet exciton hopping. An additional non-radiative decay pathway of singlet excitons was identified, in which the S_1 state forgoes SF and decays directly to the ground state. This quenching process becomes significant at small particle sizes, greatly reducing triplet yields from SF. To the best of our knowledge, this is the first report of such a non-SF singlet quenching mechanism in acene NPs. These significant variations of exciton dynamics with particle size account for quantitative discrepancies in the literature for amorphous TIPS-Pn, hence indicating the importance of considering particle size in interpreting results of NP models for SF-capable chromophores such as TIPS-Pn.

Supporting Information Description

(1) Characterization of nanoparticle size by dynamic light scattering, (2) additional steady-state and time-resolved fluorescence data, (3) extraction of exciton basis spectra, (4) spectral deconvolution of transient absorption spectra, (5) estimated singlet fission yield losses due to triplet pair decay, (6) estimation of exciton diffusion lengths, (7) kinetic fits to all nanoparticle sizes, (8) excitation density- and surface charge density-dependent transient absorption experiments, (9) kinetic fitting without non-radiative singlet decay, and (10) modelling non-radiative singlet exciton decay as a surface-quenching phenomenon.

Acknowledgements

This work was supported by an Australian Government Research Training Program (RTP) scholarship and funding from the Australian Research Council (DP160103797 and LE0989747). The authors also thank Dr. Patrick Tapping for discussions that contributed to this work.

References

(1) Smith, M. B.; Michl, J. Recent Advances in Singlet Fission. *Annu. Rev. Phys. Chem.* **2013**, *64*, 361–386.

(2) Kim, H.; Zimmerman, P. M. Coupled Double Triplet State in Singlet Fission. *Phys. Chem. Chem. Phys.* **2018**, *20*, 30083–30094.

(3) Miyata, K.; Conrad-Burton, F. S.; Geyer, F. L.; Zhu, X.-Y. Triplet Pair States in Singlet Fission. *Chem. Rev.* **2019**, *119*, 4261–4292.

(4) Dexter, D. L. Two Ideas on Energy Transfer Phenomena: Ion-Pair Effects Involving the OH Stretching Mode, and Sensitization of Photovoltaic Cells. *J. Lumin.* **1979**, *18-19*, 779–784.

(5) Tayebjee, M. J. Y.; Gray-Weale, A. A.; Schmidt, T. W. Thermodynamic Limit of Exciton Fission Solar Cell Efficiency. *J. Phys. Chem. Lett.* **2012**, *3*, 2749–2754.

(6) Tayebjee, M. J. Y.; McCamey, D. R.; Schmidt, T. W. Beyond Shockley–Queisser: Molecular Approaches to High-Efficiency Photovoltaics. *J. Phys. Chem. Lett.* **2015**, *6*, 2367–2378.

(7) Congreve, D. N.; Lee, J.; Thompson, N. J.; Hontz, E.; Yost, S. R.; Reusswig, P. D.; Bahlke, M. E.; Reineke, S.; Van Voorhis, T.; Baldo, M. A. External Quantum Efficiency Above 100% in a Singlet-Exciton-Fission–Based Organic Photovoltaic Cell. *Science* **2013**, *340*, 334–337.

(8) Rao, A.; Friend, R. H. Harnessing Singlet Exciton Fission to Break the Shockley-Queisser Limit. *Nat. Rev. Mater.* **2017**, *2*, 17063.

(9) Lee, J.; Jadhav, P.; Reusswig, P. D.; Yost, S. R.; Thompson, N. J.; Congreve, D. N.; Hontz, E.; Van Voorhis, T.; Baldo, M. A. Singlet Exciton Fission Photovoltaics. *Acc. Chem. Res.* **2013**, *46*, 1300–1311.

(10) Gish, M. K.; Pace, N. A.; Rumbles, G.; Johnson, J. C. Emerging Design Principles for Enhanced Solar Energy Utilization with Singlet Fission. *J. Phys. Chem. C* **2019**, *123*, 3923–3934.

(11) Felter, K.; Grozema, F. C. Singlet Fission in Crystalline Organic Materials: Recent Insights and Future Directions. *J. Phys. Chem. Lett.* **2019**, *10*, 7208–7214.

(12) Ullrich, T.; Munz, D.; Guldi, D. M. Unconventional Singlet Fission Materials. *Chem. Soc. Rev.* **2021**, *50*, 3485–3518.

(13) Hetzer, C.; Guldi, D. M.; Tykwinski, R. R. Pentacene Dimers as a Critical Tool for the Investigation of Intramolecular Singlet Fission. *Chem. Eur. J.* **2018**, *24*, 8245–8257.

(14) Anthony, J. E.; Brooks, J. S.; Eaton, D. L.; Parkin, S. R. Functionalized Pentacene Improved Electronic Properties from Control of Solid-State Order. *J. Am. Chem. Soc.* **2001**, *123*, 9482–9483.

(15) Diao, Y.; Lenn, K. M.; Lee, W.-Y.; Blood-Forsythe, M. A.; Xu, J.; Mao, Y.; Kim, Y.; Reinspach, J. A.; Park, S.; Aspuru-Guzik, A. et al. Understanding Polymorphism in Organic Semiconductor Thin Films through Nanoconfinement. *J. Am. Chem. Soc.* **2014**, *136*, 17046–17057.

(16) Jones, A. C.; Kearns, N. M.; Ho, J.-J.; Flach, J. T.; Zanni, M. T. Impact of Non-Equilibrium Molecular Packings on Singlet Fission in Microcrystals Observed using 2D White-Light Microscopy. *Nat. Chem.* **2020**, *12*, 40–47.

(17) Doucette, G. S.; Huang, H.-T.; Munro, J. M.; Munson, K. T.; Park, C.; Anthony, J. E.; Strobel, T.; Dabo, I.; Badding, J. V.; Asbury, J. B. Tuning Triplet-Pair Separation versus Relaxation Using a Diamond Anvil Cell. *Cell Rep. Phys. Sci.* **2020**, *1*, 100005.

(18) Pensack, R. D.; Tilley, A. J.; Parkin, S. R.; Lee, T. S.; Payne, M. M.; Gao, D.; Jahnke, A. A.; Oblinsky, D. G.; Li, P.-F.; Anthony, J. E. et al. Exciton Delocaliza-

tion Drives Rapid Singlet Fission in Nanoparticles of Acene Derivatives. *J. Am. Chem. Soc.* **2015**, *137*, 6790–6803.

(19) Pensack, R. D.; Grieco, C.; Purdum, G. E.; Mazza, S. M.; Tilley, A. J.; Ostroumov, E. E.; Seferos, D. S.; Loo, Y.-L.; Asbury, J. B.; Anthony, J. E. et al. Solution-Processable, Crystalline Material for Quantitative Singlet Fission. *Mater. Horiz.* **2017**, *4*, 915–923.

(20) Pensack, R. D.; Tilley, A. J.; Grieco, C.; Purdum, G. E.; Ostroumov, E. E.; Granger, D. B.; Oblinsky, D. G.; Dean, J. C.; Doucette, G. S.; Asbury, J. B. et al. Striking the Right Balance of Intermolecular Coupling for High-Efficiency Singlet Fission. *Chem. Sci.* **2018**, *9*, 6240–6259.

(21) Stuart, A. N.; Tapping, P. C.; Schrefl, E.; Huang, D. M.; Kee, T. W. Controlling the Efficiency of Singlet Fission in TIPS-Pentacene/Polymer Composite Nanoparticles. *J. Phys. Chem. C* **2019**, *123*, 5813–5825.

(22) Grieco, C.; Doucette, G. S.; Pensack, R. D.; Payne, M. M.; Rimshaw, A.; Scholes, G. D.; Anthony, J. E.; Asbury, J. B. Dynamic Exchange During Triplet Transport in Nanocrystalline TIPS-Pentacene Films. *J. Am. Chem. Soc.* **2016**, *138*, 16069–16080.

(23) Tayebjee, M. J. Y.; Schwarz, K. N.; MacQueen, R. W.; Dvořák, M.; Lam, A. W. C.; Ghiggino, K. P.; McCamey, D. R.; Schmidt, T. W.; Conibeer, G. J. Morphological Evolution and Singlet Fission in Aqueous Suspensions of TIPS-Pentacene Nanoparticles. *J. Phys. Chem. C* **2016**, *120*, 157–165.

(24) Hudson, R. J.; de la Perrelle, J. M.; Pensack, R. D.; Kudisch, B.; Scholes, G. D.; Huang, D. M.; Kee, T. W. Organizing Crystalline Functionalized Pentacene Using Periodicity of Poly(Vinyl Alcohol). *J. Phys. Chem. Lett.* **2020**, 516–523.

(25) Hudson, R. J.; Huang, D. M.; Kee, T. W. Anisotropic Triplet Exciton Diffusion in Crystalline Functionalized Pentacene. *J. Phys. Chem. C* **2020**, *124*, 23541–23550.

(26) Kasai, H.; Nalwa, H. S.; Oikawa, H.; Okada, S.; Matsuda, H.; Minami, N.; Kakuta, A.; Ono, K.; Mukoh, A.; Nakanishi, H. A Novel Preparation Method of Organic Microcrystals. *Jpn. J. Appl. Phys.* **1992**, *31*, L1132.

(27) Chung, H.-R.; Kwon, E.; Oikawa, H.; Kasai, H.; Nakanishi, H. Effect of Solvent on Organic Nanocrystal Growth using the Reprecipitation Method. *J. Cryst. Growth* **2006**, *294*, 459–463.

(28) Mori, J.; Miyashita, Y.; Oliveira, D.; Kasai, H.; Oikawa, H.; Nakanishi, H. Stopped-Flow Analysis on the Mechanism of Perylene Nanoparticle Formation by the Reprecipitation Method. *J. Cryst. Growth* **2009**, *311*, 553–555.

(29) de la Perrelle, J. M. Coherence and Singlet Fission of TIPS-Pentacene Probed by Two-dimensional Electronic Spectroscopy. M.Sc. thesis, Department of Chemistry, The University of Adelaide, Adelaide, SA, 2021.

(30) Fu, H.-B.; Yao, J.-N. Size Effects on the Optical Properties of Organic Nanoparticles. *J. Am. Chem. Soc.* **2001**, *123*, 1434–1439.

(31) Kurokawa, N.; Yoshikawa, H.; Hirota, N.; Hyodo, K.; Masuhara, H. Size-Dependent Spectroscopic Properties and Thermochromic Behavior in Poly(substitutedthiophene) Nanoparticles. *ChemPhysChem* **2004**, *5*, 1609–1615.

(32) Mauck, C. M.; Hartnett, P. E.; Wu, Y.-L.; Miller, C. E.; Marks, T. J.; Wasielewski, M. R. Singlet Fission within Diketopyrrolopyrrole Nanoparticles in Water. *Chem. Mater.* **2017**, *29*, 6810–6817.

(33) Aragó, J.; Viruela, P. M.; Ortí, E.; Malavé Osuna, R.; Hernández, V.; López Navarrete, J. T.; Swartz, C. R.; Anthony, J. E. Functionalized Pentacenes: A Combined Theoretical, Raman and UV–Vis Spectroscopic Study. *Theor. Chem. Acc.* **2011**, *128*, 521–530.

(34) Ramanan, C.; Smeigh, A. L.; Anthony, J. E.; Marks, T. J.; Wasielewski, M. R. Competition between Singlet Fission and Charge Separation in Solution-Processed Blend Films of 6,13-Bis(triisopropylsilylethynyl)pentacene with Sterically-Encumbered Perylene-3,4:9,10-bis(dicarboximide)s. *J. Am. Chem. Soc.* **2012**, *134*, 386–397.

(35) Munson, K. T.; Gan, J.; Grieco, C.; Doucette, G. S.; Anthony, J. E.; Asbury, J. B. Ultrafast Triplet Pair Separation and Triplet Trapping following Singlet Fission in Amorphous Pentacene Films. *J. Phys. Chem. C* **2020**, *124*, 23567–23578.

(36) Grieco, C.; Doucette, G. S.; Munson, K. T.; Swartzfager, J. R.; Munro, J. M.; Anthony, J. E.; Dabo, I.; Asbury, J. B. Vibrational Probe of the Origin of Singlet Exciton Fission in TIPS-pentacene Solutions. *J. Chem. Phys.* **2019**, *151*, 154701.

(37) Lee, T. S.; Lin, Y. L.; Kim, H.; Pensack, R. D.; Rand, B. P.; Scholes, G. D. Triplet Energy Transfer Governs the Dissociation of the Correlated Triplet Pair in Exothermic Singlet Fission. *J. Phys. Chem. Lett.* **2018**, *9*, 4087–4095.

(38) Zhou, Z.; Ma, L.; Guo, D.; Zhao, X.; Wang, C.; Lin, D.; Zhang, F.; Zhang, J.; Nie, Z. Ultrafast Dynamics of Long-Lived Bound Triplet Pair Generated by Singlet Fission in 6,13-Bis(triisopropylsilylethynyl) Pentacene. *J. Phys. Chem. C* **2020**, *124*, 14503–14509.

(39) van Stokkum, I. H. M.; Larsen, D. S.; van Grondelle, R. Global and Target Analysis of Time-Resolved Spectra. *Biochim. Biophys. Acta Bioenerg.* **2004**, *1657*, 82–104.

(40) Yong, C. K.; Musser, A. J.; Bayliss, S. L.; Lukman, S.; Tamura, H.; Bubnova, O.; Hallani, R. K.; Meneau, A.; Resel, R.; Maruyama, M. et al. The Entangled Triplet Pair State in Acene and Heteroacene Materials. *Nat. Commun.* **2017**, *8*, 15953.

(41) Marciniak, H.; Pugliesi, I.; Nickel, B.; Lochbrunner, S. Ultrafast Singlet and Triplet Dynamics in Microcrystalline Pentacene Films. *Phys. Rev. B* **2009**, *79*, 235318.

(42) Han, J.; Xie, Q.; Luo, J.; Deng, G.-H.; Qian, Y.; Sun, D.; Harutyunyan, A. R.; Chen, G.; Rao, Y. Anisotropic Geminate and Non-Geminate Recombination of Triplet Excitons in Singlet Fission of Single Crystalline Hexacene. *J. Phys. Chem. Lett.* **2020**, *11*, 1261–1267.

(43) Prasad, J.; Kopelman, R. A New Technique to Differentiate Between Geminate and Nongeminate Recombination of Triplet Excitons. *J. Lumin.* **1990**, *45*, 258–259.

(44) Kosco, J.; Bidwell, M.; Cha, H.; Martin, T.; Howells, C. T.; Sachs, M.; Anjum, D. H.; Gonzalez Lopez, S.; Zou, L.; Wadsworth, A. et al. Enhanced Photocatalytic Hydrogen Evolution from Organic Semiconductor Heterojunction Nanoparticles. *Nat. Mater.* **2020**, *19*, 559–565.

(45) Pustulka, K. M.; Wohl, A. R.; Lee, H. S.; Michel, A. R.; Han, J.; Hoye, T. R.; McCormick, A. V.; Panyam, J.; Macosko, C. W. Flash Nanoprecipitation: Particle Structure and Stability. *Mol. Pharmaceutics* **2013**, *10*, 4367–4377.

(46) Olaya-Castro, A.; Scholes, G. D. Energy Transfer from Förster–Dexter Theory to Quantum Coherent Light-Harvesting. *Int. Rev. Phys. Chem.* **2011**, *30*, 49–77.

(47) Yost, S. R.; Hontz, E.; Yeganeh, S.; Van Voorhis, T. Triplet vs Singlet Energy Transfer in Organic Semiconductors: The Tortoise and the Hare. *J. Phys. Chem. C* **2012**, *116*, 17369–17377.

(48) Turro, N. J.; Ramamurthy, V.; Scaiano, J. *Principles of Molecular Photochemistry*; University Science Books: Sausalito, California, USA, 2009.

(49) Schweitzer, C.; Schmidt, R. Physical Mechanisms of Generation and Deactivation of Singlet Oxygen. *Chem. Rev.* **2003**, *103*, 1685–1758.

(50) Wollscheid, N.; Pérez Lustres, J. L.; Kefer, O.; Hahn, S.; Brosius, V.; Bunz, U. H. F.;

Motzkus, M.; Buckup, T. Oxygen-Catalysed Sequential Singlet Fission. *Nat. Commun.* **2019**, *10*, 5202.

(51) Ishibashi, Y.; Arinishi, M.; Katayama, T.; Miyasaka, H.; Asahi, T. Excited-State Dynamics of Fullerene Nanoparticles Dispersed in Pure Water. *Chem. Lett.* **2012**, *41*, 1104–1106.

TOC Graphic

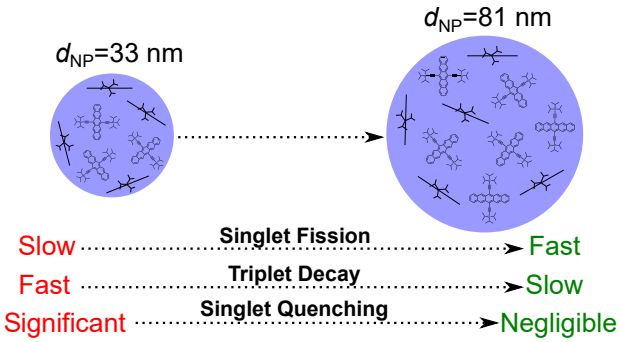
d_{NP}=33 nm
d_{NP}=81 nm
Slow
Singlet Fission
Fast
Fast
Triplet Decay
Slow
Significant
Singlet Quenching
Negligible